DINAME 2019 - Proceedings of the XVIII International Symposium on Dynamic Problems of Mechanics,
M.A. Savi, T.G. Ritto and W.M. Bessa (Editors), ABCM, Buzios, RJ, Brazil, March 10th to 15th, 2019

Friction coefficient influence on the nonlinear dynamics of a drill-string experimental model with stick-slip

Bruno C. Cayres[1,2]**, and Hans I. Weber**[1]

[1] Pontifícia Universidade Católica do Rio de Janeiro, 225 Marquês de São Vicente Street, Gávea - Rio de Janeiro, RJ - Brazil, hans@puc-rio.br

[2] Centro Federal de Educação Tecnológica Celso Suckow da Fonseca, Mario Covas Avenue, Santana - Itaguaí, RJ - Brazil, bruno.cayres@cefet-rj.br

Abstract: Because of diameter-to-length ratio of the drilling system, torsional vibration mode is present in most drilling processes and may reach an undesired severe stage: stick-slip phenomenon. The stick-slip phenomenon is the main source of component failures during drilling process and may excite other vibration modes. In this work, the nonlinear behavior of an experimental apparatus simulating drill-string in reduced scale is approached. The lumped parameters technique is used to achieve the equations of motion. The nonlinearity rises from the adopted dry friction model which simulates the bit-rock interactions. Numerical and experimental results are compared in order to validate the mathematical model. Subsequently, the local stability analysis is performed using Hurwitz criterion: the equilibrium branches and the torsional map are found. One may observe that the limit points experience Hopf bifurcations. The limit cycles are found numerically. For this, the reference angular velocity is used as bifurcation parameter. Basins of attraction also indicate the coexistence of both stable equilibrium and limit cycle for a range of the bifurcation parameter. The kinetic coefficient of friction is modified and its influence is analyzed.

Keywords: ***Nonlinear analysis, stick-slip phenomenon, drill-string experimental set-up, dry friction-induced vibrations***

INTRODUCTION

Because of diameter-to-length ratio of the drilling system, torsional vibration mode is present in most drilling processes and may reach an undesired severe stage: stick-slip. This stage consists of a complete arrest of the drill-bit (stick phase), while the top continues rotating and storing elastic torsional energy in the drill-string. Suddenly, the energy stored overcomes the friction torque and the drill-bit is released to rotate (slip phase) - converting potential energy into kinetic energy. The stick-slip phenomenon occurs approximately 50% of the total drilling time (Kriesels et al., 1999 apud Patil and Teodoriu, 2013) and it is the main source of component failures during drilling process. Also it may excite axial vibration in its severe way: bit-bounce (Saldivar et al., 2011). According to Patil and Teodoriu (2013) the torsional vibrations while drilling is one of the severe types of drill-string vibration which deteriorates the overall drilling performance, causing damages of the bit, failure of bottom-hole assembly (BHA), torsional fatigue of drill-string, and excites other vibration modes.

This work aims to investigate the nonlinear behavior of a experimental set-up simulating a drill-string system. The torsional vibration mode was isolated and the stick-slip phenomenon was observed. The mathematical model used was compared with experimental data in Cayres et al. (2018). The brake device which creates friction in the the test rig possesses the possibility of changing the material responsible for the friction. Keeping in mind this material change possibility, which may lead to different coefficients of friction, we varied the kinetic coefficient of friction in order to investigate its influence on the response of the system numerical model.

MATHEMATICAL MODEL OF THE TEST RIG

The experimental set-up is thoroughly described in Cayres et al. (2018). The test rig is shown in Fig. 1. Figure 2 illustrates a schematic diagram of the test rig. The system is composed by a DC-motor which provides torque to the mechanical part. This latter consists of a low-stiffness shaft and two discs: Disc 1 (R_1) and Disc 2 (R_2) have the mass moments of inertia J_1 and J_2, respectively. The system may be modeled as described in Eq. (1).

$$\begin{aligned} J_1\ddot{\theta}_1 + d_1\left(\dot{\theta}_1 - \dot{\theta}_2\right) + k_1\delta_{12} + T_{r_1}\left(\dot{\theta}_1\right) &= 0 \\ J_2\ddot{\theta}_1 + d_1\left(\dot{\theta}_2 - \dot{\theta}_1\right) + d_2\left(\dot{\theta}_2 - \dot{\theta}_3\right) + k_2\delta_{23} - k_1\delta_{12} + T_{r_2}\left(\dot{\theta}_2\right) &= 0 \\ d_2\left(\dot{\theta}_3 - \dot{\theta}_2\right) - k_2\delta_{23} &= \eta\left(K_T\, i - C_m\eta\,\dot{\theta}_3 - T_f - J_m\eta\,\ddot{\theta}_3\right) \\ L\frac{\mathrm{d}i}{\mathrm{d}t} + R\,i + K_E\,\eta\,\dot{\theta}_3 &= u. \end{aligned} \tag{1}$$

The stiffnesses are denoted by k_1 and k_2, as well as d_1 and d_2 denote the damping. The angular displacements,

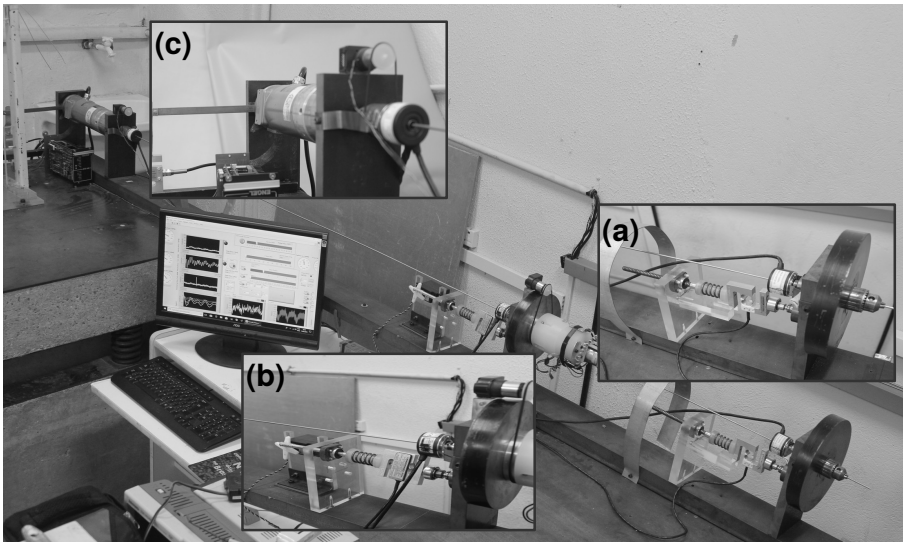

Figure 1 – Drill-string experimental set-up. (a) Disc 1 (R_1) and brake device 1, (b) Disc 2 (R_2) and brake device 2 and (c) DC-motor (Cayres et al., 2018).

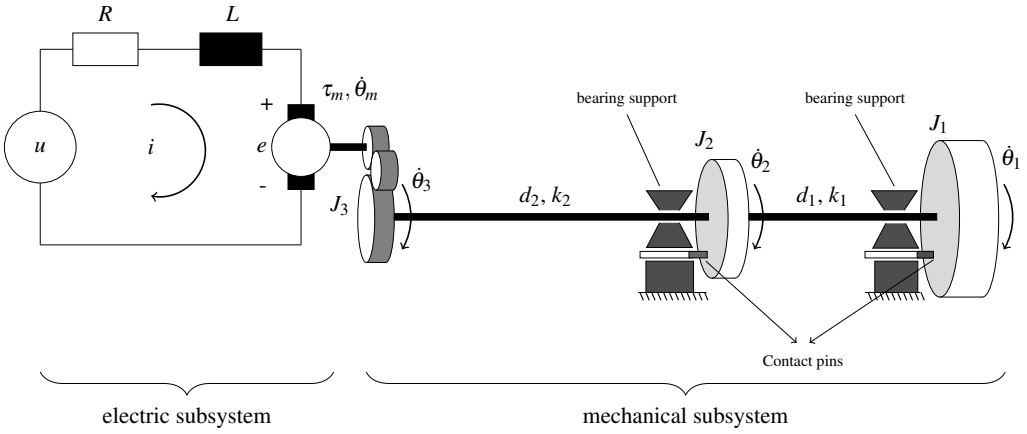

Figure 2 – Schematic diagram of the test bench (Pereira et al., 2018).

velocities and accelerations are denoted by θ_i, $\dot{\theta}_i$ and $\ddot{\theta}_i$ for $i = 1,2,3$, respectively. The angular displacements are denoted by $\delta_{12} = \theta_1 - \theta_2$ and $\delta_{23} = \theta_2 - \theta_3$. The electric current of the DC-motor is denoted by i. L and R are the armature inductance and resistance, respectively. The angular velocity $\dot{\theta}_m$ is the velocity of the inertia of the DC-motor J_m. C_m and K_T are the speed regulation and constant torque of the motor, respectively. Further, K_E consists of the voltage constant and T_f is the internal friction torque. The input voltage is denoted by u. The relation between the subsystem are $\dot{\theta}_m = \eta\,\dot{\theta}_3$ and $\eta = 8$. Therewith, $J_3 = \eta^2 J_m$. From Eq. (1), the system may be rewritten as state space formulation. The following equations (Eqs. (2) and (3)) show the state variables and state equations, respectively

$$\mathbf{x} = \begin{bmatrix} \theta_1 - \theta_2 \\ \theta_2 - \theta_3 \\ \dot{\theta}_1 \\ \dot{\theta}_2 \\ \dot{\theta}_3 \\ i \end{bmatrix} = \begin{bmatrix} x_1 \\ x_2 \\ x_3 \\ x_4 \\ x_5 \\ x_6 \end{bmatrix}, \tag{2}$$

$$\begin{aligned}
\dot{x}_1 &= x_3 - x_4 \\
\dot{x}_2 &= x_4 - x_5 \\
\dot{x}_3 &= \left[-d_1 x_3 + d_1 x_4 - k_1 x_1 - T_{r_1}(x_3)\right]/J_1 \\
\dot{x}_4 &= \left[d_1 x_3 - (d_1 + d_2) x_4 - d_2 x_5 + k_1 x_1 - k_2 x_2 - T_{r_2}(x_4)\right]/J_2 \\
\dot{x}_5 &= \left[k_2 x_2 - (\eta^2 C_m + d_2) x_5 + d_2 x_4 + \eta K_T x_6 - \eta T_f\right]/J_3 \\
\dot{x}_6 &= \left[-R x_6 - \eta K_E x_5 + u\right]/L,
\end{aligned} \tag{3}$$

Following, the resistive torque is expressed as (Mihajlović et al., 2004; Vromen, 2015; Liu et al., 2017)

$$T_{r_1}(\dot{\theta}_1) = N_1 r_1 \left[\mu_k + (\mu_s - \mu_k)\cdot e^{-\mathrm{v_b}|\dot{\theta}_1|}\right]\cdot \mathrm{sign}\left(\dot{\theta}_1\right), \tag{4}$$

where r_1 is the distance between the contact point of the pin and the geometric center of rotation of disc R_1, N_1 is the normal force applied on R_1, μ_s and μ_k are the static and kinetic coefficients of friction, $\mathrm{v_b} = 1$ is a decay factor. In order to avoid numerical discontinuity in Eq. (3), the friction model in Eq. (4) is rewritten as follows (Thomsem, 1999)

$$T_{r_1}(\dot{\theta}_1) = N_1 r_1 \begin{cases} \mu_s \dot{\theta}_1/\omega_s & for \quad |\dot{\theta}_1| < \omega_s \\ \left[\mu_k + (\mu_s - \mu_k)\cdot e^{-\mathrm{v_b}|\dot{\theta}_1|}\right]\cdot \mathrm{sign}\left(\dot{\theta}_1\right) & for \quad |\dot{\theta}_1| \geq \omega_s \end{cases}, \tag{5}$$

where $\omega_s = 10^{-3}$. Figure 3 graphically illustrates the

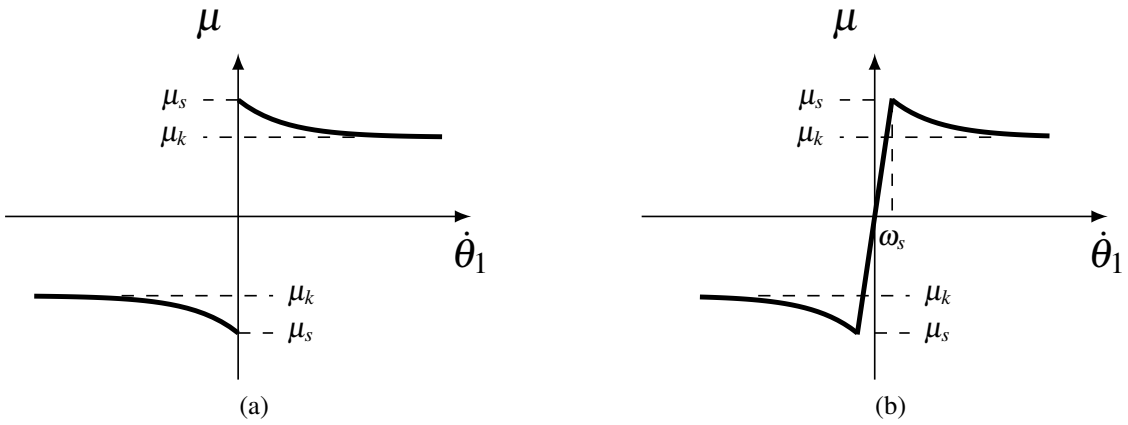

Figure 3 – Friction model (a) with discontinuity represented by Eq. (4)**, and (b) without discontinuity represented by Eq.** (5)**.**

The DC-motor presents a PI internal controller which is responsible to maintain the angular velocity of the motor. Herein, this input voltage may be expressed as

$$u = k_p\left(\omega_{ref} - x_5\right) + k_i \int_0^t \left(\omega_{ref} - x_5\right)\mathrm{d}t \tag{6}$$

where k_p and k_i are the proportional and integral constants, ω_{ref} is the reference angular velocity in rad/s. This relation in Eq. (6) maintains the idea of a desired angular speed that is imposed by an operator.

The system behavior during stick-slip is compared in Fig. 4. This latter illustrates the similar behavior of the numerical and experimental models. The electrical and mechanical parameters used in simulations are described in Tabs. 1 and 2, respectively.

Table 1 – Electrical parameters of DC-motor.

Parameter	Description	Value	Unit
L	Armature inductance	$8.437 * 10^{-4}$	H
R	Armature resistance	0.33	Ω
K_T	Torque constant	0.126	Nm/A
K_E	Voltage constant	0.0602	$V/(rad/s)$
T_f	Friction torque	0.1196	Nm
C_m	Speed regulation constant	$1.784 * 10^{-4}$	$Nm/(rad/s)$
k_p	proportional constant	2.800	–
k_i	integral constant	3.500	–

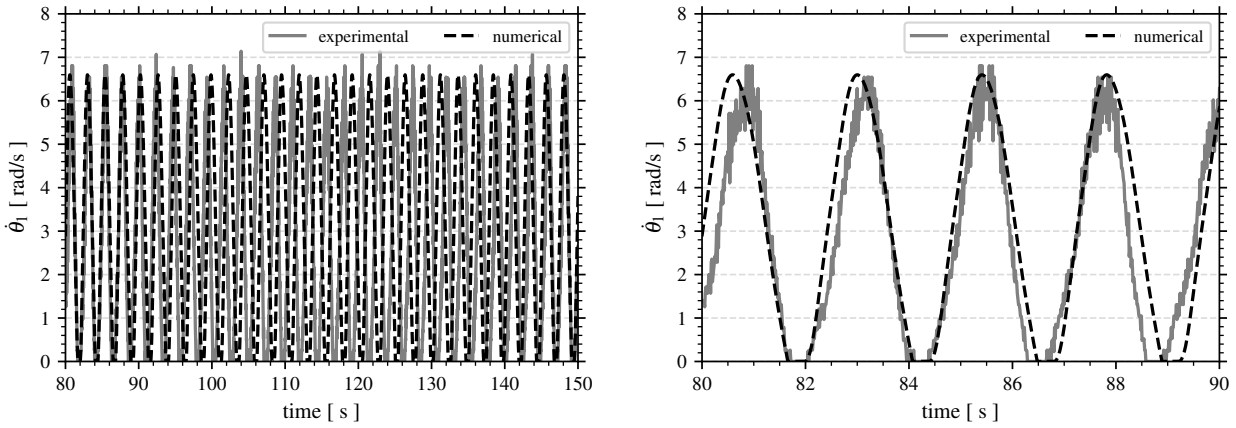

Figure 4 – Test rig response for $3.14\ rad/s$ **(**$30\ rpm$**) with (a) stick-slip and (b) stick-slip zoomed.** $N_1 = 25.0$ **N and** $T_{r_2} = 0.0$ **Nm. Continuous gray and dashed black lines contain experimental and numerical results, respectively (Cayres et al., 2018).**

Table 2 – Mechanical parameters of test rig.

Parameter	Description	Value	Unit
J_1	R_1 moment of inertia	0.0288	kgm^2
J_2	R_2 moment of inertia	0.0149	kgm^2
J_3	DC-motor moment of inertia	0.0237	kgm^2
k_1	stiffness between R_1-R_2	1.1175	Nm/rad
k_2	stiffness between R_2-Motor	0.3659	Nm/rad
d_1	damping between R_1-R_2	0.0202	Nms/rad
d_2	damping between R_2-Motor	0.0167	Nms/rad
μ_s	static friction coefficient	0.47	–
μ_k	kinetic friction coefficient	0.30	–
v_b	decay factor	0.978	s/rad

STABILITY ANALYSIS

The qualitative structure of motion, considered as a dynamic flow, can change when certain parameters vary. Therewith, stable solutions can be created or destroyed, or become unstable. Stable equilibrium points or trajectories (all discs with the same angular velocity ω_{ref}) and stable limit cycles (torsional vibration at the discs) were observed in the experimental set-up. Thereby, these behavior sets are addressed.

Equilibrium points

Reminding that the test bench system described by Eq. (1) presents nonlinearities rising from the friction torque model on R_1, and at the moment, there is no torque applied on Disc 2 (R_2), so that $T_{r_2} = 0.0$ Nm. For the analytical and stability analysis, the resistive torque described by Eq. 4 is used. Therewith, in the equilibrium points it holds that $\left(\delta_{12}, \delta_{23}, \dot{\theta}_1, \dot{\theta}_2, \dot{\theta}_3, i\right) = \left(\delta_{12}^*, \delta_{23}^*, \omega^*, \omega^*, \omega^*, i^*\right)$ and $u = u_c$ so that u_c is a constant. Also, $\delta_{12} = \theta_1 - \theta_2$ and $\delta_{23} = \theta_2 - \theta_3$. Thereby, Eq. (1) becomes

$$\begin{aligned} k_1\,\delta_{12}^* + T_{r_1}(\omega^*) &= 0, \\ k_2\,\delta_{23}^* - k_1\,\delta_{12}^* &= 0, \\ C_m\eta^2\,\omega^* - k_2\,\delta_{23}^* &= \eta K_T\,i^* - \eta T_f, \\ R\,i^* + \eta K_E\,\omega^* &= u_c. \end{aligned} \tag{7}$$

The third equation of (7) means a torque balance of the electro-mechanical system:

$$C_m \eta^2 \omega^* + T_{r_1}(\omega^*) + \eta T_f = \eta K_T i^*, \tag{8}$$

where the right side means the provided torque and the left side the loss torques. Also, one may verify the equilibrium point as

$$\begin{array}{rcl} \delta_{12}^* & = & \frac{-T_{r_1}(\omega_1^*)}{k_1}, \\ \delta_{23}^* & = & \frac{-T_{r_1}(\omega^*)}{k_2}, \\ i^* & = & \frac{u_c - \eta K_E \omega^*}{R}. \end{array} \tag{9}$$

Local stability analysis

In order to analyze the local stability for $\omega_{ref} > \omega_{min}$, the system is linearized around an equilibrium point. First, Eq. 3 is rewritten as follows

$$\begin{array}{l} \dot{x}_1 = x_3 - x_4 \\ \dot{x}_2 = x_4 - x_5 \\ \dot{x}_3 = \left[-d_1 x_3 + d_1 x_4 - k_1 x_1 - T_{r_1}(x_3)\right]/J_1 \\ \dot{x}_4 = \left[d_1 x_3 - (d_1 + d_2) x_4 - d_2 x_5 + k_1 x_1 - k_2 x_2 - T_{r_2}(x_4)\right]/J_2 \\ \dot{x}_5 = \left[k_2 x_2 - (\eta^2 C_m + d_2) x_5 + d_2 x_4 + \eta K_T x_6 - \eta T_f\right]/J_3 \\ \dot{x}_6 = \left[-R x_6 - \eta K_E x_5 + k_p(\omega_{ref} - x_5) + k_i x_7\right]/L, \\ \dot{x}_7 = \omega_{ref} - x_5, \end{array} \tag{10}$$

and the Jacobian matrix around an equilibrium $\mathbb{J}^*$ may be performed.

$$\mathbb{J}^* = \left[\frac{\partial \dot{x}_i}{\partial x_j}\right] \tag{11}$$

Herein, ΔT_{r_1} is defined as

$$\Delta T_{r_1} = \left.\frac{\mathrm{d}T_{r_1}}{\mathrm{d}\dot{\theta}_1}\right|_{\dot{\theta}_1 = \omega^*}. \tag{12}$$

The characteristic polynomial of the matrix $\mathbb{J}^*$ is presented as follows

$$\lambda^7 + a_1\lambda^6 + a_2\lambda^5 + a_3\lambda^4 + a_4\lambda^3 + a_5\lambda^2 + a_6\lambda + a_7 = 0. \tag{13}$$

Therewith, the Hurwitz criterion is applied. Herein, all the Δ_i are polynomials as functions of ΔT_{r_1}. Therefore, one may state that the equilibrium point of the system is asymptotically stable for

$$\Delta T_{r_1} > \Delta T_{r_{min}} \tag{14}$$

where $\Delta T_{r_{min}} = \max(\Delta T_{\Delta_i})$, and ΔT_{Δ_i} is the largest real part of the roots of the polynomial Δ_i for $i = 1, 2, ..., 7$. For the system parameters (Tabs. 1 and 2), we obtain

$$\Delta T_{r_{min}} = -0.0128 \quad \frac{Nms}{rad}. \tag{15}$$

Figure 5(a) illustrates the following case: $N_1 = 10.0$ N, the system is locally stable for $\dot{\theta}_1 > 1.994\ rad/s$. For $\dot{\theta}_1 < 1.994\ rad/s$, the stability is not ensured. In addition, Figure 5(b) shows the case that $N_1 = 20.0$ N, the system is locally stable for $\dot{\theta}_1 > 2.689\ rad/s$, and for $\dot{\theta}_1 < 2.689\ rad/s$, the system is unstable, according to Hurwitz criterion. As one may also verify in Fig. 5, the negative slope of the friction model may be crucial to the stable solution. The coefficient of kinetic friction μ_k is 0.3.

Using the performed stability analysis so far, the equilibrium set expressed by Eq. (9) is illustrated in Fig. 6. Before the minimum angular velocity ω_{min}, there exists a stable equilibrium branch which means that the system remains still (not enough torque to overcome the losses). Thereafter, the equilibrium branch becomes locally unstable. For speeds above the critical velocity observed in Fig. 5, the equilibrium branch becomes stable again.

The torsional vibration map (TVM) may also be obtained (Cayres et al., 2018) via Hurwitz criterion (Leipholz, 1970; Franca, 2004; Navarro-López and Suárez, 2004) using $\mu_k = 0.3$. Figure 7(a) illustrates two zones: one with stable periodic

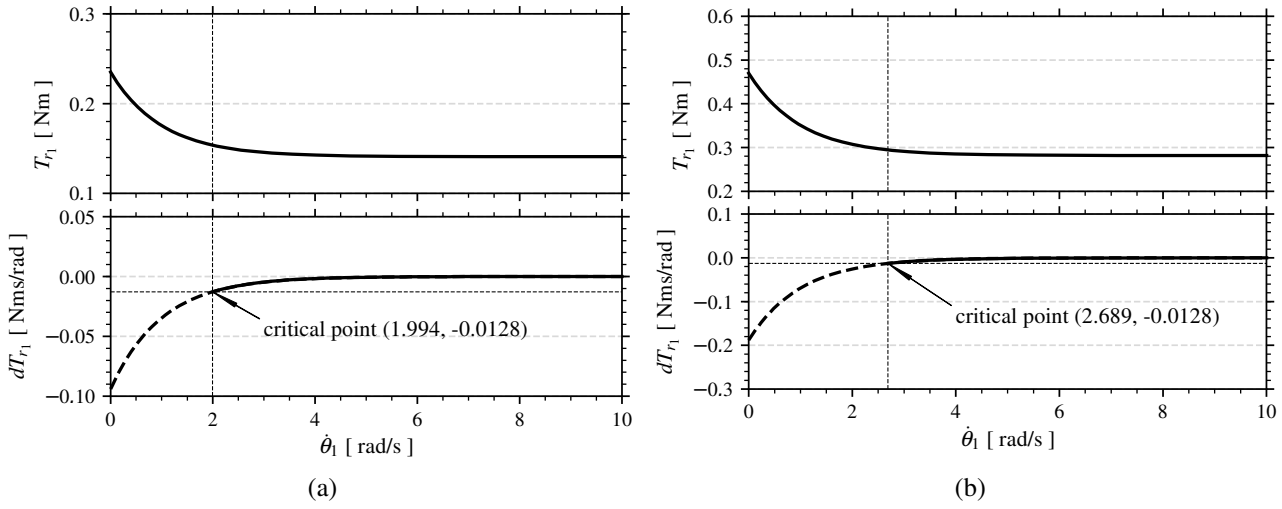

Figure 5 – Graphic illustration of the local stability analysis via Hurwitz criterion for (a) $N_1 = 10.0\ N$**, and (b)** $N_1 = 20.0\ N$**. Continuous and dashed lines mean asymptotically local stable and unstable, respectively,** $\mu_k = 0.3$ **and** $T_{r_2} = 0.0\ Nm$**.**

solutions and the other with equilibrium solutions (Nayfeh and Balachandran, 2008). This means that in the left side of the curve, the system undergoes torsional vibrations (upper Fig. 7(b)) and, in the right side, it presents no vibration (lower Fig. 7(b)).

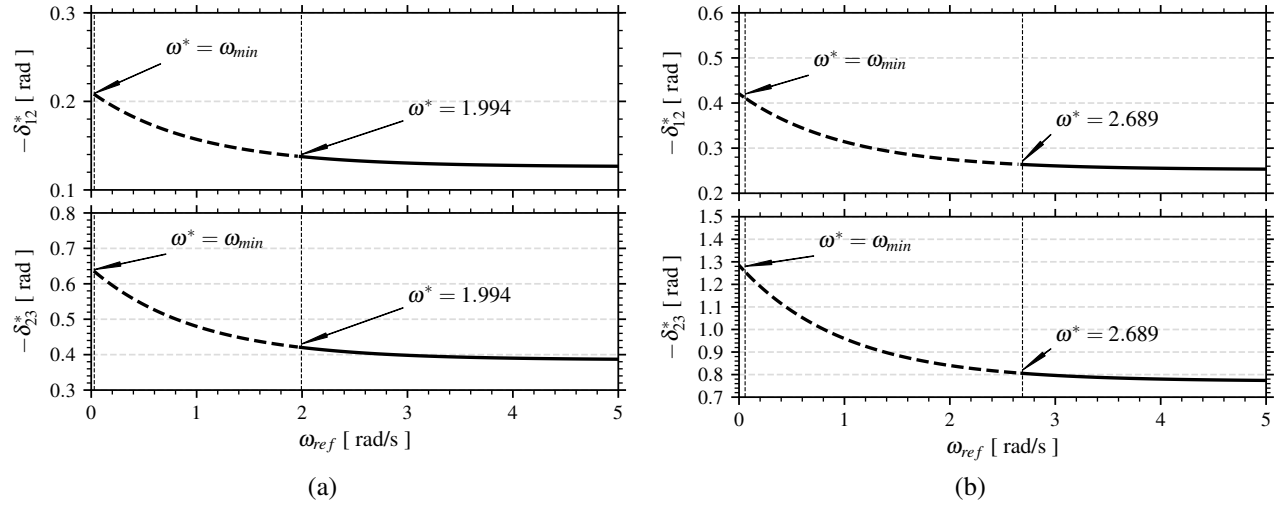

Figure 6 – Local stability analysis of the equilibrium branch (Eq. (9)) via Hurwitz criterion for (a) $N_1 = 10.0\ N$**, and (b)** $N_1 = 20.0\ N$**. Continuous and dashed lines mean locally stable and unstable branches, respectively,** $\mu_k = 0.3$ **and** $T_{r_2} = 0.0\ Nm$**.**

INFLUENCE OF COEFFICIENT OF KINETIC FRICTION μ_K

In the previous section, we identify stable and unstable equilibrium branches of the system. However, the friction proprieties may change over some circumstances, such as lithology, rock variation or/and bit wear.

Herein, we perform an analysis of the influence of the friction on the stability of the system. The coefficient of kinetic friction μ_k is increased 0.3 up to 0.375 while the coefficient of static friction one is kept constant $\mu_s = 0.47$. The former value ($\mu_k = 0.3$) was identified in Cayres et al. (2018) for the test rig (Fig. 1). Figure 8 shows different curve for each μ_k value.

We observe that the system performs equilibrium and periodic solutions depending on the reference angular velocity ω_{ref}. The limit cycles and equilibria are numerically obtained via `PyDSTool` package (Clewley et al., 2008). The bifurcation diagram is performed for different values of μ_k. The maximum values of the angular velocity of the Disc 1 (R_1) is plotted when a periodic solution is found, while the normal force N_1 is kept constant (Fig. 9(a)). In this figure, a supercritical Hopf bifurcation occurs in $\omega_{ref} \approx 0.0$ rad/s, and stable periodic branches arise while an unstable equilibrium branch appears (the dashed line of θ_1 varying linearly with ω_{ref}). Thereafter, the periodic solution amplitudes

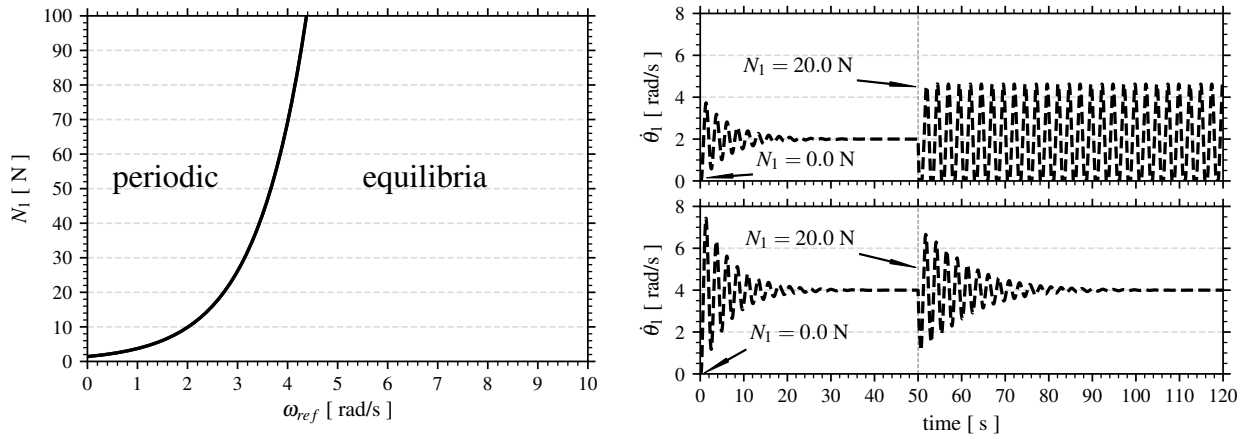

Figure 7 – (a) Torsional vibration map and (b) time response of the Disc 1 (R_1) for $2\ rad/s$ **(upper) and** $4\ rad/s$ **(lower).** $N_1 = 0.0\ N$ **at** $0 < t < 50$ **and** $N_1 = 20.0\ N$ **at** $t > 50$**,** $\mu_k = 0.3$ **and** $T_{r_2} = 0.0\ Nm$ **(Cayres et al., 2018).**

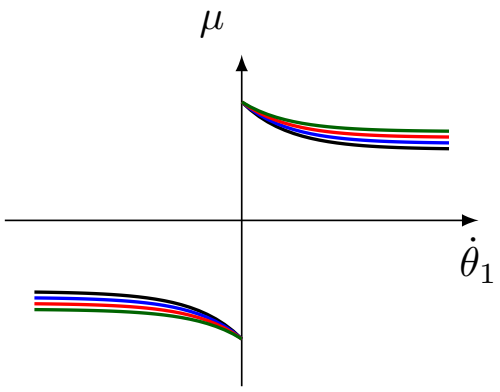

Figure 8 – Representation of the friction model (Eq. (4)**) for —** $\mu_k = 0.300$**; —** $\mu_k = 0.325$**; —** $\mu_k = 0.350$**; and —** $\mu_k = 0.375$**.**

increase with the increase of ω_{ref} and then there exists an unstable periodic branch and subcritical Hopf bifurcation occurs. Subsequently, a stable equilibrium branch arises (no torsional vibration). Figure 9(b) illustrates the torsional vibration map for different values of μ_k. From this graphs, we conclude that the vibration amplitude reduces when μ_k approaches μ_s. Also, the equilibrium branch arises earlier for bigger μ_k value compared to smaller μ_k value. Furthermore, the equilibrium zone is bigger for $\mu_k = 0.375$ than $\mu_k = 0.30$.

In a situation that the coefficient of kinetic friction is very close to the static friction ($\mu_k \approx \mu_s$), the system presents only equilibrium zone (or a very small periodic solution zone) as we may see in Fig. 10(a). Equation (4) now represents a Coulomb friction model as we may observe in upper Fig. 10(b). Lower Fig. 10(b) illustrates, according to Eq. (12), that the equilibrium branch is stable for all reference angular velocity domain ω_{ref}.

The plane portraits and the time response of the numerical model are depicted in Fig. 11. Figure 11(a) illustrates the $\dot{\theta}_1$ amplitudes decrease with increase of μ_k. However, more evident is the variation of the static equilibrium point represented by the displacement of the orbits to the left until it becomes a dot in the chart ($\mu_k = 0.465 \approx \mu_s$). The time response for each adopted value of μ_k is depicted in Fig. 11(b) - except for $\mu_k = 0.3$ which was illustrated in Fig. 7(b). The brown dot in the Fig. 11(a) is a straight line in Fig. 11(b), presenting no torsional oscillation. Figures 11(c) and (d) depict the angular displacement difference δ_{12} as function of time: in these graphs the decrease in oscillation amplitudes is more evident when μ_k increases.

CONCLUSIONS

An experimental apparatus simulating a drill-string system was developed and the torsional behavior was isolated. A low-stiffness shaft transmits rotational motion from DC-motor to two discs with moments of inertia J_1 and J_2 - Disc 1 (R_1) and Disc 2 (R_2). In the former, we applied a friction torque in order to induce torsional vibration, whereas in the latter we did not apply any torque.

Experimental observations have proved the existence of stick-slip phenomenon for a given combination of normal

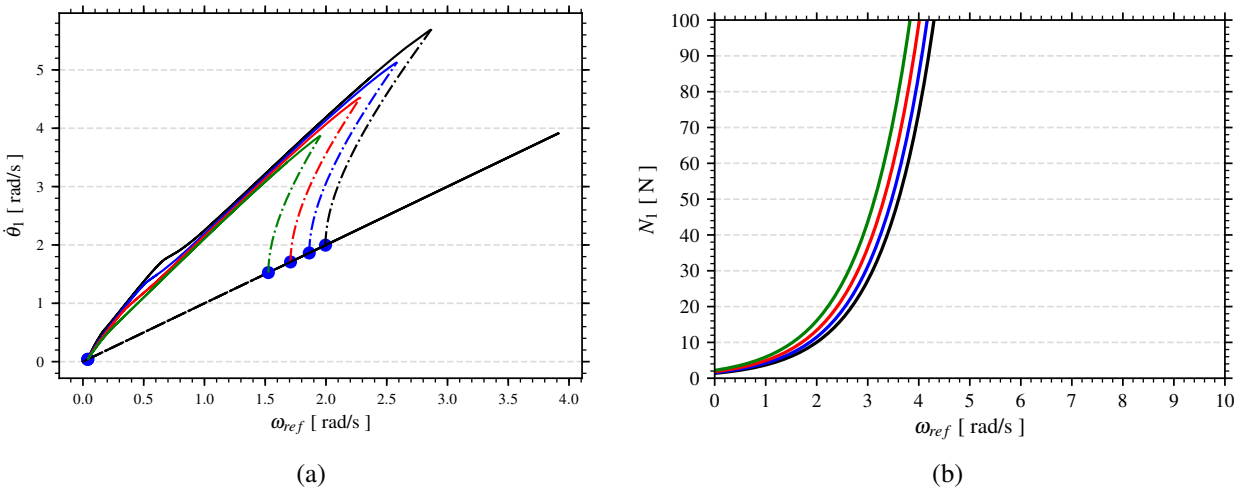

(a) (b)

Figure 9 – (a) Numerical bifurcation diagram of the experimental set-up model with maximum value of $\dot{\theta}_1$ for $N_1 = 10.0\ N$, and (b) the torsional vibration map. In (a) the continuous and dashed lines represent stable and unstable solutions, respectively, and $T_{r_2} = 0.0\ Nm$. The values for the coefficient of kinetic friction are — $\mu_k = 0.300$; — $\mu_k = 0.325$; — $\mu_k = 0.350$; and — $\mu_k = 0.375$.

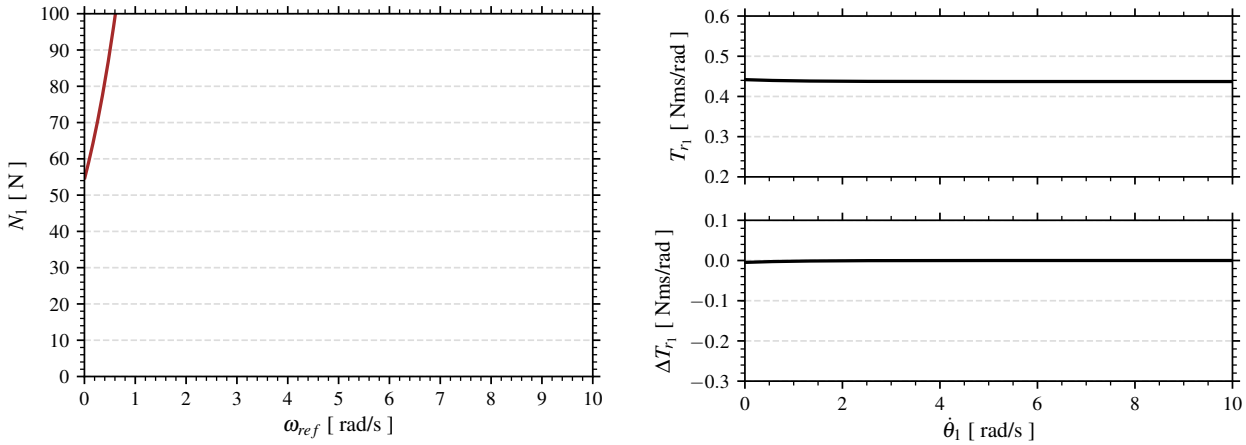

(a) (b)

Figure 10 – Local stability analysis via Hurwitz criterion: (a) Torsional vibration map, and (b) Eqs. (4) **and** (12)**.** —$\mu_k = 0.465$ **(**$\approx \mu_s$**).** $N_1 = 20\ N$ **and** $T_{r_2} = 0.0\ Nm$**.**

force (N_1) and reference angular velocity (ω_{ref}). The brake device which creates friction in the the test rig possesses the possibility of changing the material responsible for the friction (for a more detailed description of the experimental apparatus see Cayres (2018)). Therewith, the coefficients of friction also may change.

In this work, we used the compared and validated numerical model (see Cayres et al., 2018) to investigate the influence of different kinetic coefficients of friction μ_k on the dynamics of the system. About the friction model, we may state that the friction slope is substantially linked to the stability of the system solutions. In fact, some researchers show the system instability in a range of the bifurcation parameter equivalent to the negative slope of the friction model (Mihalović, 2005; Kang et al., 2009). We also observed this statement in Figs. 5 and 6.

The maximum amplitudes of the system in the bifurcation diagram become smaller as μ_k approaches μ_s and the periodic solution zone reduces (Fig. 9). An ultimate case that $\mu_k = \mu_s$, the friction model becomes the Coulomb friction model and no instability is observed in the equilibrium branches according to Hurwitz criterion. Therefore, we may conclude that the Coulomb friction model does not provide stick-slip phenomenon in the system. One could propose to increase the normal force N_1, but if we do increase it the system will continue to rotate with no torsional oscillation. If we increase N_1 up to a value for the which the Disc 1 does not rotate while the DC-motor continues to impose torque, the shaft would deform permanently (deformations bigger than the deformations of elastic linear region assumed in the model). Physically, this is because we considered that the DC-motor has an angular velocity regulator which maintains (or tries to) the reference angular velocity (ω_{ref}) constant - the internal PI controller usual in torque providers.

As already stated, the slope of the friction model is extremely important to model stick-slip in the system. The slope is

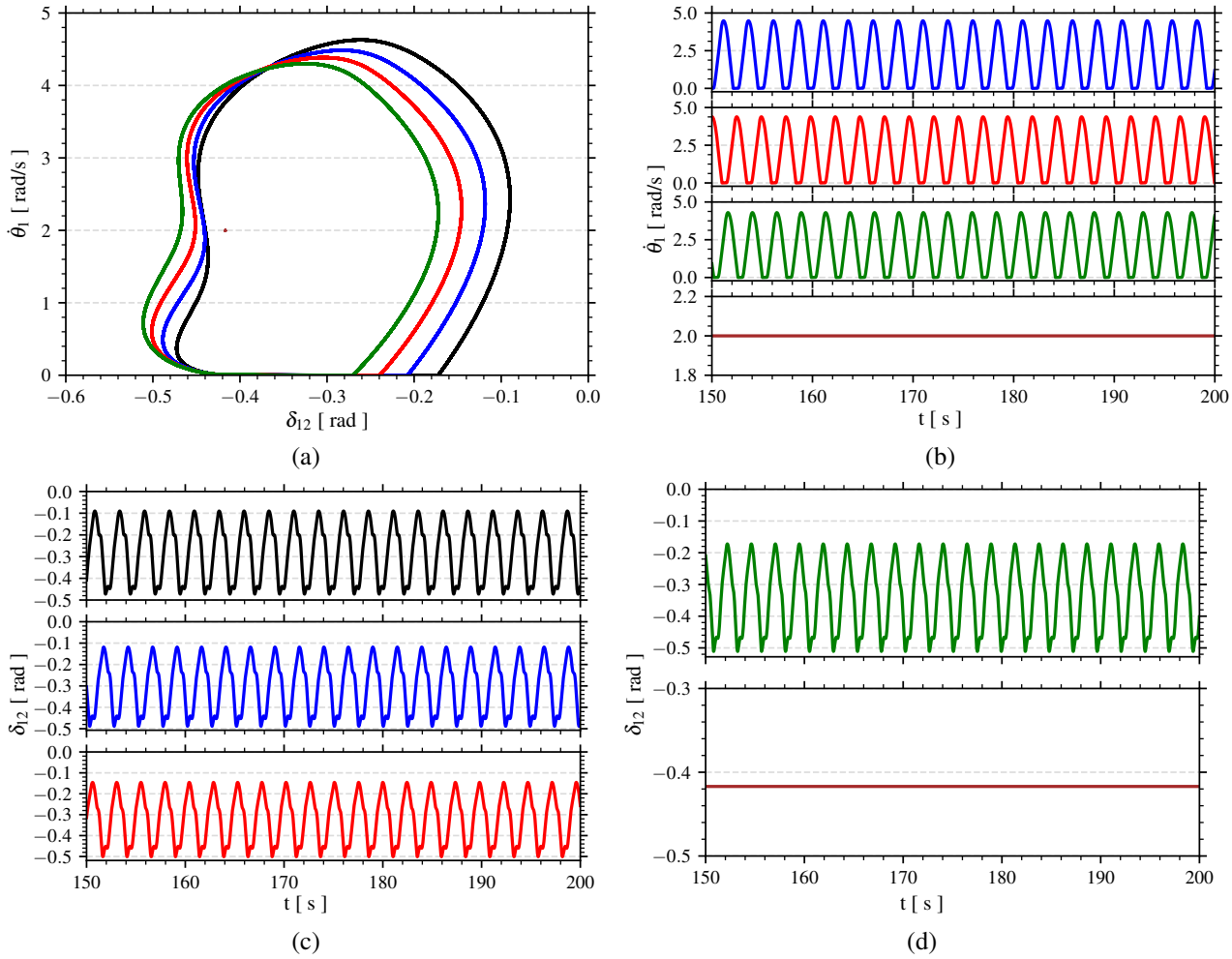

Figure 11 – (a) Plane portraits and (b) time response of the numerical model for — $\mu_k = 0.300$**; —** $\mu_k = 0.325$**; —** $\mu_k = 0.350$**; —** $\mu_k = 0.375$**; and —** $\mu_k = 0.465$**.** $N_1 = 20\ N$**,** $\omega_{ref} = 2.0\ rad/s$**, and** $T_{r_2} = 0.0\ Nm$**.**

referenced as weakening velocity effect which provides a "trap zone" of vibrations, creating a periodic solution attractor. This effect is responsible for the self-sustained vibration characteristic in this sort of system.

REFERENCES

Cayres, B.C., Fonseca, C.A., Sampaio, G., Weber, H.I., 2018, "Analysis of a drill-string experimental set-up with dry friction-induced torsional vibration", Proceedings of the 10th International Conference on Rotor Dynamics - IFToMM, , MMS 62, pp. 1-14.

Cayres, B.C., 2018, "Nonlinear dynamic analysis of dry friction-induced torsional vibration in a drill-string experimental set-up", D.Sc. thesis, Pontifícia Universidade Católica do Rio de Janeiro, Rio de Janeiro, Brazil.

Clewley, R.; Sherwood, E.; LaMar, D.; Guckenheimer, J., 2008, "PyDSTool: a software environment for dynamical systems modeling", http://sourceforge. net/projects/pydstool.

Franca, L.F.P., 2004, "Self-Excited Percussive-Rotary Drilling in Hard Rockss", D.Sc. thesis, Pontifícia Universidade Católica do Rio de Janeiro, Rio de Janeiro, Brazil.

Kang, J.; Krousgrill, C.M.; Sadeghi, F., 2009, "Oscillation pattern of stick–slip vibrations", International Journal of Non-Linear Mechanics, Vol. 44, No. 7, pp. 820–828.

Kriesels, P.C., Keultjes, W.J., Dumont, P., Huneidi, I., Owoeye, O.O. and Hartmann, R.A., 1999, "Cost savings through an integrated approach to drillstring vibration control", SPE/IADC Middle East Drilling Technology Conference.

Leipholz, H., 1970, "Stability theory: An introduction to the stability of dynamic systems and rigid bodies", Academic Press.

Liu, Y., Chávez, J.P., Sa, R., Walker, S., 2017, "Numerical and experimental studies of stick-slip oscillations in drill-string", Nonlinear Dynamics, Vol. 90, No. 4, pp. 2959-2978.

Mihalović, N., Van Veggel, A.A., Van de Wouw, N., Nijmeijer, H., 2004, "Analysis of friction-induced limit cycling in an experimental drill-string system", Journal of Dynamic Systems, Measurement and Control, Vol. 126, pp. 709720.

Mihajlović, N., 2005, "Torsional and Lateral Vibrations in Flexible Rotor Systems with Friction", D.Sc. thesis, Eindhoven University of Technology, Eindhoven, Netherlands.

Navarro-López, E.M.; Suárez, R., 2004, "Modelling and analysis of stick-slip behaviour in a drillstring under dry friction", Congress of the Mexican Association of Automatic Control, pp. 330-335.

Nayfeh, A.H.; Balachandran, B., 2008, "Applied nonlinear dynamics: analytical, computational and experimental methods", John Wiley & Sons.

Patil, P.A. and Teodoriu, C., 2013, "Model development of torsional drillstring and investigating parametrically the stick-slips influencing factors", Journal of Energy Resources Technology, Vol. 135, No. 1, pp. 13-103.

Pereira, L.D., Cayres, B.C., Weber, H.I., 2018, "Numerical application of a stick-slip control and experimental analysis using a test rig", MATEC Web of Conferences, Vol. 148.

Salvivar, B., Mondié, S., Loiseau, J.J., Rasvan, V., 2014, "Suppressing axial-torsional coupled vibrations in drillstrings", Journal of Control Engineering and Applied Informatics, Vol. 15, No. 1, pp. 3-10.

Thomsem, J.J., 1999, "Using fast vibrations to quench friction-induced oscillations", Journal of Sound and Vibration, Vol. 228, No. 5, pp. 1079–1102.

Vromen, T.G.M., 2015, "Control of stick-slip vibrations in drilling systems", D.Sc. Thesis, Eindhoven University of Technology, Eindhoven, Netherlands.

RESPONSIBILITY NOTICE

The authors are the only responsible for the printed material included in this paper.